INVITED REVIEW

Modeling defect cluster evolution in irradiated structural materials: Focus on comparing to high-resolution experimental characterization studies

Brian D. Wirth[a] and Xunxiang Hu
Department of Nuclear Engineering, University of Tennessee, Knoxville, Tennessee 37996-2300, USA; and Oak Ridge National Laboratory, Oak Ridge, Tennessee 37831, USA

Aaron Kohnert and Donghua Xu
Department of Nuclear Engineering, University of Tennessee, Knoxville, Tennessee 37996-2300, USA

(Received 13 October 2014; accepted 8 January 2015)

It is well established that exposure of metallic structural materials to irradiation environments results in significant microstructural evolution, property changes, and performance degradation, which limits the extended operation of current generation light water reactors and restricts the design of advanced fission and fusion reactors. Further, it is well recognized that these irradiation effects are a classic example of inherently multiscale phenomena and that the mix of radiation-induced features formed and the corresponding property degradation depend on a wide range of material and irradiation variables. This inherently multiscale evolution emphasizes the importance of closely integrating models with high-resolution experimental characterization of the evolving radiation-damaged microstructure. This article provides a review of recent models of the defect microstructure evolution in irradiated body-centered cubic materials, which provide good agreement with experimental measurements, and presents some outstanding challenges, which will require coordinated high-resolution characterization and modeling to resolve.

I. INTRODUCTION

Exposure of metallic structural materials to irradiation environments results in significant microstructural evolution, property changes, and performance degradation, which limits the extended operation of current generation light water reactors and restricts the design of advanced fission and fusion reactors.[1–8] This effect of irradiation on materials' microstructure and properties is a classic example of an inherently multiscale phenomenon, as schematically illustrated in Fig. 1(a). Pertinent processes range from the atomic nucleus to structural component length scales, spanning more than 15 orders of magnitude. Time scales bridge more than 22 orders of magnitude, with the shortest being less than a femtosecond.[1,8] Further, the mix of radiation-induced features formed and the corresponding property degradation depend on a wide range of material and irradiation variables. This emphasizes the importance of closely integrating models with high-resolution experimental characterization of the evolving radiation-damaged microstructure, including measurements performed in situ during irradiation. In this article, we review some recent successes through the use of closely coordinated modeling and experimental studies of the defect cluster evolution in irradiated body-centered cubic materials, followed by a discussion of outstanding challenges still to be addressed, which are necessary for the development of comprehensive models of radiation effects in structural materials.

At the smallest scales (nanometer and picosecond), radiation damage continually initiates with the creation of energetic primary knock-on atoms in (primarily) elastic collisions between high-energy neutrons and lattice atoms.[1,8] Specifically for fusion conditions, there is also the production of high concentrations of transmutants, including insoluble He and H gas, produced in (n,α) and (n,p) neutron capture reactions, many of which have threshold energies above several MeV and thus are not typically produced in fission neutron irradiations.[2–5] The primary knock-on atoms and recoiling transmutant nuclei quickly lose their kinetic energy in a chain of subsequent atomic collision displacements, generating a cascade of vacancy and self-interstitial defects. High-energy displacement cascades evolve over very short times, $\sim$100 picoseconds or less, and small volumes, with characteristic length scales of 50 nm or less, and are directly amenable to molecular dynamics (MD) simulations. The physics of primary damage production in high-energy displacement cascades has been extensively studied with MD simulations.[8–14] The key conclusions of the high-energy (>20 keV) simulations are that

Contributing Editor: William J. Weber
[a]Address all correspondence to this author.
e-mail: bdwirth@utk.edu
DOI: 10.1557/jmr.2015.25

https://doi.org/10.1557/jmr.2015.25 Published online by Cambridge University Press

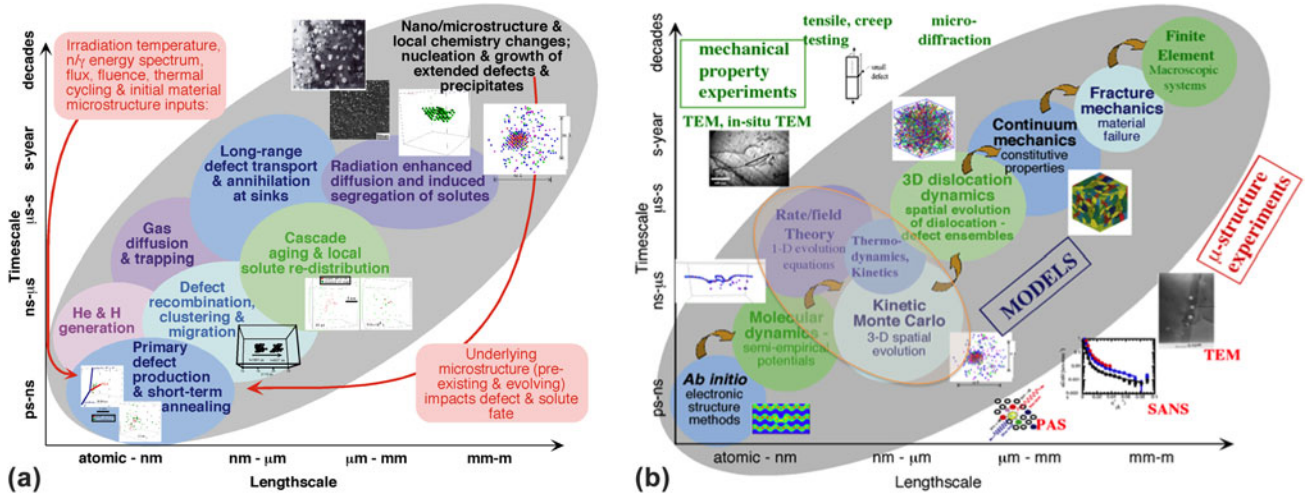


FIG. 1. (a) Illustration of the length and time scales (and feedback) involved in the multiscale processes responsible for microstructural changes in irradiated materials. (b) Illustration of an integrated experimental and computational science-based approach to the multiscale investigation of materials degradation due to high-energy particle irradiation, in which the light orange ellipse highlights the microstructural simulation techniques of OKMC and mean-field reaction-diffusion CD rate theory models, which are the primary focus of this article.

(i) intracascade recombination of vacancies and self-interstitial atoms (SIA) results in ~25–30% of the defect production expected from displacement theory, (ii) many-body collision effects produce a spatial correlation (separation) of the vacancy and self-interstitial defects, (iii) substantial clustering of the self-interstitials and to a lesser extent, the vacancies occurs within the cascade volume, and (iv) high-energy displacement cascades tend to break up into lobes, or subcascades, which may either enhance recombination (thereby decreasing damage production) or increase damage through the interaction of supersonic shock fronts for cascade energy divided by displacement energy above about 300.

Spatial correlations continue to play an important role in nano/microstructural development, as the defects produced in the cascade at 100 ps evolve, or age, over much longer time scales.[1,8] The cascade aging evolution is governed by the time and temperature dependent kinetics of defect diffusion, clustering, and annihilation. Fortunately, separation between the diffusion time scales of vacancies and SIA/SIA clusters naturally leads to the nearly independent evolution of these two populations, at least for relatively low dose rates and low doses, before cascade overlap becomes important. For example, numerous MD studies have shown that the SIA clusters in body-centered cubic iron are directly produced in high-energy displacement cascades and undergo one-dimensional glide with very low activation energies of ≤0.1 eV.[15–17] This low activation energy is contrasted to a value about 0.25 eV for individual SIA, which is higher than for the one-dimensionally migrating clusters in computational studies due to the higher activation energy associated with rotations and translations for the three-dimensionally migrating single SIA, and a value between about 0.6 and 1.0 eV for vacancies. Thus, mobile loops and isolated self-interstitials quickly diffuse through the vacancy debris and leave the cascade region. The additional vacancy–self-interstitial re-combination that occurs during this phase of cascade aging has been modeled with kinetic Monte Carlo (KMC) methods.[18]

The evolution of the remaining vacancy rich cascade core in Fe, and more recently in tungsten, has also been modeled by KMC methods,[18–22] in the limit of infinitesimal dose rate. Within ms, most of the cascade vacancies jump short distances to form small, compact three-dimensional clusters, while a small fraction leave the cascade region. Subsequently, the vacancy clusters migrate, coarsen, and ultimately dissolve. From these KMC studies, it was observed that the reduction of the net residual vacancy concentration in the cascade core by emission–migration–annihilation events was essentially continuous in the model, but progressively slowed with cluster growth. Vacancy clusters initially grew through the coalescence of smaller mobile clusters, and later by emission–absorption processes. Notably, the formation of small (10–30) vacancy clusters, which are not visible in the transmission electron microscope (TEM), has been confirmed in positron annihilation spectroscopy measurements in Fe and Fe–Cu alloys irradiated at temperatures below ~300 °C.[23,24]

The vacancy mediated cascade aging described in the preceding paragraph is limited to infinitesimal dose-rates and intermediate to low irradiation temperatures around 300 °C. Clearly, the timescale associated with vacancy cluster coarsening and dissolution processes, as well as the assumption related to separation of the SIA/vacancy evolution timescales depends on the details of point defect interactions with solutes, impurities, precipitate interfaces, and extended defects like dislocations, in

https://doi.org/10.1557/jmr.2015.25 Published online by Cambridge University Press

addition to depending strongly on irradiation temperature. As but one example, solute/impurity binding with small vacancy clusters as well as the segregation of chemical impurities (including He and possibly also hydrogen) to the surface of nanometer-sized voids leads to increased vacancy cluster/nanovoid thermal stability. A quantitative assessment of vacancy/nanovoid-impurity complex lifetime, in particular, with He and/or H transmutants, and the coupled interactions amongst point defect clusters, solutes, impurities, and extended defects within the higher operating temperatures proposed for advanced fission reactors and in the fusion environment remains an outstanding issue.

Ultimately, long-range diffusion of vacancy and self-interstitial defects that escape the cascade region is responsible for nano/microstructural evolution. Enhanced defect transport leads to a re-distribution of solute and impurity elements as a consequence of radiation enhanced diffusion and segregation. Solute re-distribution can alter the local chemistry and result in the precipitation of phases not expected within a homogeneously distributed alloy. Outstanding questions relate to the effect of cascade aging processes on the fraction of defects contributing to long-range diffusion; the interaction of diffusing defects with continuously generated cascade debris; the modification of defect clustering and diffusion processes as a result of interactions with an evolving underlying nano/microstructure; and the efficiency of various microstructural sinks (including dislocations, grain boundaries, nanoscale precipitate interfaces, and defect clusters themselves) in point defect cluster annihilation, including the effect of sink evolution resulting from defect annihilation.

The clustering, diffusion, and ultimate annihilation of the vacancies, self-interstitials, and point defect clusters occur over timescales from nanoseconds to well in excess of seconds, as discussed in the preceding paragraphs, and alter the local chemistry and internal structure at the nanometer and micrometer length scale. Solutes and impurities are re-distributed as a consequence of radiation enhanced diffusion and radiation induced segregation processes, and the evolving local chemical environment will also influence the defect transport kinetics and mechanisms through a variety of trapping interactions. Notably, while many of these interactions have been postulated, the atomistic interaction mechanisms remain to be quantified through modeling and focused experimental studies. Changes in nano/microstructure defect structure and local chemical arrangements are known to be responsible for dimensional instabilities, such as swelling and irradiation creep, and mechanical property degradation, including irradiation hardening, decreased work hardening, increased susceptibility to creep rupture, and localized deformation, which impact component performance, reliability, and ultimately, lifetime.

For example, it is well established that the effect of irradiation on ferritic/martensitic alloys at low to intermediate temperatures ($T < \approx 450$ °C) is to increase yield stress, reduce strain hardening capacity, and initiate flow localization at lower strains.[1–5,25–35] The predominant microstructural features observed in TEM studies are very small (~nm) cluster-type features, which may include dislocation loops, cavities, and regions of solute segregation, as well as second phase precipitates.[26–35] The balance of these features depends on the synergistic interaction of key irradiation, material, and environmental variables, including irradiation temperature, dose and dose rate, helium production, and alloy composition. And thus, a comprehensive model that predicts the radiation damaged microstructures, with a quantitative assessment of the mix of features formed based on the key irradiation and metallurgical variables and indeed, the detailed mechanisms of their formation, as well as their precise character and composition, remain outstanding questions. The remainder of this article will describe the use of cluster dynamics (CD) and object kinetic Monte Carlo (OKMC) models, informed within a multiscale modeling methodology and closely coupled to experimental characterization of radiation-damaged body-centered cubic materials, which have successfully predicted the defect microstructure evolution in molybdenum, iron, and iron-chrome based ferritic–martensitic alloys. These results will be presented in Sec. III, along with a discussion of the key assumptions inherent in the mean-field reaction-diffusion based CD models, as well as the OKMC studies used to verify the mean field model. Section IV will highlight a number of areas for future research needs that can be addressed using high-resolution characterization techniques, closely coordinated with modeling studies, before the article is summarized in Sec. V.

II. MULTISCALE MODELING APPROACH APPLIED TO RADIATION DAMAGE

Figure 1(b) shows a schematic illustration of a science-based, and integrated experimental and computational modeling approach to investigate materials degradation in a nuclear fission or fusion environment, within an information passing methodology. Akin to the multiscale materials processes controlling property degradation, illustrated in Fig. 1(a), a multiscale approach is required to determine the controlling mechanisms and processes. Figure 1(b) illustrates the hierarchical multiscale modeling methodology, which integrates ab initio electronic structure calculations, MD simulations, KMC, rate theory simulations with thermodynamics and kinetics through the passing of information about the controlling physical mechanisms over the relevant length and time scales to model the fates of defects and solutes during high-energy

https://doi.org/10.1557/jmr.2015.25 Published online by Cambridge University Press

neutron irradiation and thus, predict nano/microstructural evolution. Detailed microstructural information can then used as a basis for modeling the mechanical behavior through meso (represented by 3D dislocation dynamics) and continuum scale models, which must be incorporated into fracture mechanics models at the continuum scale to predict material deformation and failure of individual reactor components, and which would provide predictive materials performance models for integrated system evaluation through finite element modeling. In this figure, individual modeling techniques are identified in a series of linked process ellipses, with representative schematics illustrating the type of modeled material behavior through the length and timescales. The passing of information between the scales is represented through a series of arrows. Of course, multiscale modeling by itself is insufficient to fully predict the performance of complicated engineered structures in the nuclear fission or fusion environment, and the science-based multiscale paradigm involves a close integration with a suite of experimental characterization techniques. A subset of these techniques is represented for microstructural characterization on the lower side of the gray sphere and for experimental mechanical behavior/testing methods on the upper side.

Due to space limitations, in this article we will focus entirely on the microstructural (or mesoscale) modeling of defect cluster evolution in irradiated materials using mean field reaction-diffusion CD models, which are an extension of the classical rate theory model of radiation damage, and with cross-comparison for model verification through the use of OKMC simulations. This region of the multiscale materials modeling paradigm shown in Fig. 1(b) has therefore been highlighted with an orange ellipse. In the remainder of this section, we do not fully describe the range of models illustrated within Fig. 1(b), but rather we will focus on a succinct description of the CD and KMC models that are the focus of the work described here. Further description of these CD and KMC models is available in Refs. 36–46.

A. CD model based on reaction-diffusion rate theory

Isolated vacancies and SIA, as well as three-dimensional vacancy clusters and clusters of SIA in the form of planar, prismatic dislocation loops are continuously formed and will evolve in pure body-centered cubic iron under neutron irradiation.[9–11,15,36,47,48] A CD model based on the reaction-diffusion rate theory is used here to predict the evolution of the vacancy and SIA defect clusters, which is a modified version of the model developed by Xu and Wirth[36–39] and only considers the intrinsic defects and their clusters. Furthermore, since the probability that SIA and vacancy co-exist in a single cluster is very low due to their strong tendency for recombination, no mixed I–V clusters are considered, and it is thus sufficient to define any cluster using just an integer, with its absolute value being the number of point defects contained in the complexes and its sign ("−" for SIA clusters, or "+" for V-clusters) indicating the character of the cluster. Two numbers, NI and NV, are chosen as the number of interstitials in the largest SIA-cluster and the number of vacancies in the largest V-cluster, respectively. Physically, these numbers prescribe the "phase space" within which the clusters can interact with each other and ensure the conservation of point defects. NI and NV should be chosen sufficiently large so that the computational results are not impacted by a prescribed phase space that is too small (e.g., insufficient cluster size to allow growth to large defect cluster size).

For neutron irradiation, it is common to model the system without a discrete spatial dependence, making use of the mean field approximation, as described here. However, for many cases of ion irradiation, and in particular for thin-film ion irradiation studies, the spatial dependence of the damage profile and the strong influence of the free surfaces require an explicit spatial dependence in the model, as fully described in Refs. 36–39 and 41–43. As well, the nature of defect generation in metals induced by ions and neutrons is significantly different. The energy transfer cross-section for ion–atom collisions is an atomic cross-section ($\sim 10^{-17}$ cm^2) while that for neutrons is a nuclear cross-section ($\sim 10^{-24}$ cm^2), and consequently, neutrons have a much larger range between collisions when traveling in a material. The damage production varies weakly along the depth direction for neutron irradiation and therefore, it is reasonable to treat the distribution of radiation damage production as homogeneous.[40] Thus, as noted previously, no explicit spatial dimension is necessary in this model, at least for low neutron dose levels before a clear spatial correlation of the defect microstructure develops.

Without an explicit spatial dependence, the concentration of each cluster is only a function of time, and ordinary differential equations describe the defect evolution. The binary reactions discussed in Refs. 36–40, 47, and 48 are still appropriate and become simpler, because there are only two types of defects (V- and SIA-clusters) considered during neutron irradiation. The generic form to describe the evolution of a cluster, without spatial dependence, is

$$\frac{dC_i}{dt} = \phi \times P_i + G_T + G_E - A_T - A_E \quad , \qquad (1)$$

where C_i refers to the volumetric concentration (in 1/m^3) of the ith cluster, φ is the neutron flux (in neutron/m^2/s), P_i is the production "probability" of the ith cluster by neutron irradiation, G refers to the collective generation

https://doi.org/10.1557/jmr.2015.25 Published online by Cambridge University Press

rates, in which *G_T* refers to generation by trapping reactions and *G_E* refers to generation by emission, *A_T* indicates the annihilation of cluster C_i by trapping reaction events, and *A_E* refers to annihilation by emission events. The detailed construction of the coupled system of ordinary differential equations (ODEs) is thus (for which $\Lambda = [-\mathrm{NI}, \mathrm{NV}]$ is the prescribed phase space, and for which we sum over clusters $m + p = i$ for forward reactions and m reacts with i in trapping reactions to reduce the concentration of species i):

$$\frac{dC_i}{dt} = \phi \times P_i + \sum_{\substack{m+p=i \\ m,p \neq 0 \\ m,p \in \Lambda}} k^+_{m,p} C_m C_p - \sum_{\substack{m \neq i \\ m \neq 0 \\ m, m+i \in \Lambda}} k^+_{m,i} C_m C_i - k^-_i C_i \quad , \tag{2}$$

for $i = \mathrm{NV}$ or $-\mathrm{NI}$,

$$\frac{dC_i}{dt} = \phi \times P_i + \sum_{\substack{m+p=i \\ m,p \neq 0 \\ m,p \in \Lambda}} k^+_{m,p} C_m C_p + k^-_{i+1} C_{i+1} - \sum_{\substack{m \neq i \\ m \neq 0 \\ m, m+i \in \Lambda}} k^+_{m,i} C_m C_i - k^-_i C_i \quad , \tag{3}$$

for $\frac{\mathrm{NV}}{2} < i < \mathrm{NV}$,

$$\frac{dC_i}{dt} = \phi \times P_i + \sum_{\substack{m+p=i \\ m,p \neq 0 \\ m,p \in \Lambda}} k^+_{m,p} C_m C_p + k^-_{i+1} C_{i+1} - \sum_{\substack{m \neq i \\ m \neq 0 \\ m, m+i \in \Lambda}} k^+_{m,i} C_m C_i - 2k^+_{i,i} (C_i)^2 - k^-_i C_i \quad , \tag{4}$$

for $2 \leq i \leq \frac{\mathrm{NV}}{2}$,

$$\frac{dC_i}{dt} = \phi \times P_i + \sum_{\substack{m+p=i \\ m,p \neq 0 \\ m,p \in \Lambda}} k^+_{m,p} C_m C_p + 2k^-_2 C_2 + \sum_{\substack{m>2 \\ m \in \Lambda}} k^-_m C_m - \sum_{\substack{m \neq i \\ m \neq 0 \\ m, m+i \in \Lambda}} k^+_{m,i} C_m C_i - 2k^+_{i,i} (C_i)^2 \quad , \tag{5}$$

for $i = 1$,

$$\frac{dC_i}{dt} = \phi \times P_i + \sum_{\substack{m+p=i \\ m,p \neq 0 \\ m,p \in \Lambda}} k^+_{m,p} C_m C_p + 2k^-_{-2} C_{-2} + \sum_{\substack{m<-2 \\ m \in \Lambda}} k^-_m C_m - \sum_{\substack{m \neq i \\ m \neq 0 \\ m, m+i \in \Lambda}} k^+_{m,i} C_m C_i - 2k^+_{i,i} (C_i)^2 \quad , \tag{6}$$

for $i = -1$,

$$\frac{dC_i}{dt} = \phi \times P_i + \sum_{\substack{m+p=i \\ m,p \neq 0 \\ m,p \in \Lambda}} k^+_{m,p} C_m C_p + k^-_{i-1} C_{i-1} - \sum_{\substack{m \neq i \\ m \neq 0 \\ m, m+i \in \Lambda}} k^+_{m,i} C_m C_i - 2k^+_{i,i} (C_i)^2 - k^-_i C_i \quad , \tag{7}$$

for $-\frac{\mathrm{NI}}{2} \leq i \leq -2$, and

$$\frac{dC_i}{dt} = \phi \times P_i + \sum_{\substack{m+p=i \\ m,p \neq 0 \\ m,p \in \Lambda}} k^+_{m,p} C_m C_p + k^-_{i-1} C_{i-1} - \sum_{\substack{m \neq i \\ m \neq 0 \\ m, m+i \in \Lambda}} k^+_{m,i} C_m C_i - k^-_i C_i \quad , \tag{8}$$

for $-\mathrm{NI} < i < -\frac{\mathrm{NI}}{2}$, where k^+ is the forward reaction rate constant and k^- is the backward reaction rate constant, having the same expressions as the classic rate theory derivations based on isotropic interactions and spherical reaction volumes as derived by Waite based on the original work of Smoluchowski,[49,50] i.e.,

https://doi.org/10.1557/jmr.2015.25 Published online by Cambridge University Press

$$k^{+}_{m,p} = 4\pi\left(r_m + r_p\right)\left(D_m + D_p\right) \quad , \tag{9}$$

$$k^{-} = k^{+} C_0 \exp\left(-\frac{E_b}{k_B T}\right) \quad , \tag{10}$$

where r_m and r_p are the trapping radii of clusters m and p, D is the diffusion coefficient of the reacting species, C_0 is the atomic number density of the iron matrix, E_b is the binding energy of a single point defect to the cluster, k_B is Boltzmann's constant, and T is the temperature. Note that for emission ($C \rightarrow A + B$), only those events in which at least one of the two products is a monomer (i.e., I or V) are considered since it is in general more energetically favorable for a cluster to emit a monomer than emit a dimer, trimer, or a larger cluster, which is consistent with previous models.[37–39]

The variations among Eqs. (2)–(8) represent the computational details in the CD modeling, which must be considered to ensure that no computational artifacts (such as nonconservation of point defects) are introduced in the results. For example, the difference between Eqs. (7) and (8) is that in Eq. (7) the interstitial clusters, I_n, where n is less than half of the preset maximum interstitial clusters size, are allowed to interact with similar sized clusters to generate a big cluster. However, in Eq. (7), this behavior is forbidden due to the fact that the resulting larger interstitial cluster would exceed the prescribed phase space. If we were able to solve an infinite number of equations/clusters in computation, this would not be necessary, but in reality, we can only solve finite, although fairly large, number of coupled equations and hence these detailed rules of computation have to be enforced.

B. OKMC model

A different computational approach, namely OKMC,[41,44] has also been used to simulate 1 MeV Kr^+ ion irradiation in thin molybdenum foils and to compare with both the spatially dependent version of the CD model as well as in situ TEM experiments. OKMC tracks the 3-D spatial position of each individual defect cluster ("object") from birth until annihilation. A cluster can be "born" through direct cascade creation, reactions between two clusters, or one parent cluster undergoing thermal emission. A cluster can be "annihilated" by the cluster changing its size as a result of capturing another cluster or thermally emitting a monomer, or jumping to free surface sink. Further, a cluster can change its position as a result of diffusive jumps. While atomistic mechanisms of diffusion and cluster reaction are considered in rate theory models, an OKMC model explicitly tracks the three-dimensional position and identity of individual defect clusters rather than imposing a *mean field* concentration/density and is thus not subject to the limiting assumptions of rate theory. In radiation damage research, OKMC has often been used to validate sink strength or rate constant formulations that are required by rate theory or CD models[51–53] in the regime where their basic assumptions stand, but the use of OKMC to follow an entire irradiation process independently has been rare due to relatively high computational cost.[54] Xu and Wirth have recently developed an OKMC code that uses a "cell" algorithm to significantly reduce unnecessary iterations in the judgment of capturing of a cluster by any other cluster.[41] The new algorithm, combined with adaptive OpenMP parallelism, allows a fairly large simulation box with a volume of 6×10^7 nm^3, which corresponds to a minimum resolvable defect density of 1.67×10^{-8} nm^{-3} (for one defect in the box).

Black-sink boundary conditions, in which all defect concentrations are set equal to zero, are enforced along one dimension of the rectangular simulation box that represents the foil depth (36, 60, 84, and 110 nm), while periodic boundary conditions are applied along the other two dimensions. Small interstitial (I) and vacancy (V) clusters, with sizes in the range from $I_1 \sim I_{20}$ and $V_1 \sim V_9$, are created randomly in the simulation box at frequencies $\nu_{C,i} = V_{box}\phi P_i$, where V_{box} is the volume of the simulation box in nm^3, φ is the ion flux in ion/(nm^2 s), and P_i is the production probability of the cluster i in 1/(ion nm) determined through MD cascade simulations[10] and SRIM recoil energy calculations,[41] as described in more detail in Ref. 55. An already existing cluster can migrate by taking random jumps at a frequency $\nu_{J,i} = \nu_{0,i}\exp[-E^{m,i}/(k_B T)]$, where $\nu_{0,i}$ is the attempt frequency and $E^{m,i}$ is the migration energy of the cluster i. The attempt frequency is related to the diffusivity prefactor D_0 as $\nu_0 = 2n \times D_0/l^2$, where l is the jump distance (taken as the nearest neighbor distance) and n is a dimensionality number (e.g., $n = 3$ for 3-D diffusion). Diffusivity prefactors and migration energies of the interstitial clusters and single vacancy are provided in Table I, with more detail provided in Ref. 36. Note that these mobility data have been optimized based on an *effective* 3-D diffusion mode

TABLE I. Optimized mobility set to describe the diffusivity (given in terms of prefactor, D_0, and activation energy, E^m, such that $D = D_0\exp(-E^m/kT)$) for interstitial clusters/loops and single vacancy in molybdenum, where n refers to the number of interstitials in the cluster of size n.

	V	I_{1-10}	I_{11-20}	$I_{n>20}$
Diffusion prefactor, D_0 (nm^2/s)	2×10^{11}	$2 \times 10^{11}/n$	$2 \times 10^{11}/n$	$2 \times 10^{11}/n^{0.7}$
Activation energy, E^m (eV)	0.9	0.1	0.1 + 0.064 (n − 10)	1.1

https://doi.org/10.1557/jmr.2015.25 Published online by Cambridge University Press

that provides a simple but sufficient representation of mixed 1-D migration and rotation for interstitial loops. For the purpose of comparing with the CD model, the effective 3-D diffusion mode is retained in this present OKMC study, although it will be interesting in the future to implement mixed 1-D migration and rotation directly. Further, an existing cluster i can also emit monomers (single interstitials or single vacancies) by thermal activation at a frequency $\nu_{E,i}$ co-determined by diffusivities and the binding energy. For example, the frequency of a V_n cluster emitting a single vacancy is $4\pi(R_{V_1} + R_{V_{n-1}})(D_{V_1} + D_{V_{n-1}}) \exp\left[-E^{b,V_n}/(k_B T)\right]/\Omega$, where R is the cluster radius, Ω is the atomic volume, and E^{b,V_n} is the binding energy. The binding energy values have been obtained by extrapolating from ab initio calculated monomer formation energy $\left(E^{f,V_1}\right)$ and di-vacancy binding energy $\left(E^{b,V_2}\right)$ (Ref. 56) through a well-accepted 2/3-power law: $E^{f,V_1} + \left(E^{b,V_2} - E^{f,V_1}\right)\left[n^{2/3} - (n-1)^{2/3}\right]/\left(2^{2/3} - 1\right)$.[15] It should be noted that another expression existing in the literature for calculating the emission frequency, namely, $\nu_{J,V_1} \exp\left[-E^{b,V_n}/(k_B T)\right]$, is not entirely appropriate for OKMC since it fails to consider all the monomers on a cluster surface attempting to break away, although it is correct for atomistic KMC. Based on the frequencies, a single event is selected at each OKMC step out of all the time-requiring events (creation/jumping/emission) and the time is incremented using the well-known residence-time algorithm (see, e.g., Ref. 57). Upon each event, the code checks for possible trapping, surface annihilation and/or translation across periodic boundaries, which are considered to occur instantaneously.

III. RESULTS OF DEFECT CLUSTER EVOLUTION IN IRRADIATED BCC MATERIALS

A. 1 MeV Kr irradiation of Mo in the intermediate voltage electron microscope (IVEM)

Xu and Wirth, working closely in parallel with the experimental investigation by Li and Kirk, have focused on developing and validating the spatially dependent reaction diffusion CD model for 1 MeV Kr^+ irradiation in thin molybdenum (Mo) foils at 80 °C.[36,41–43] Fluxes of 1.6×10^9, 1.6×10^{10}, and 1.6×10^{11} ions/cm^2/s were used and fluences of up to 5×10^{12} ions/cm^2 were reached. A large amount of data was obtained by Li and Kirk[43] in the in situ TEM experiments at the IVEM based on continuous visualization of the defect evolution from the start of the irradiation. Specifically, the defect density and sizes were obtained at many different doses (fluences) and foil thicknesses (~10 to ~100 nm) at all three fluxes. The observed defects were confirmed to be dislocation loops with an average of ~77% possessing a Burgers vector of ½<111> and ~23% possessing <100>.

While not shown here, the spatially dependent CD model, which was parameterized based on the use of radiation damage produced in the form of only single vacancy and self-interstitials as isolated Frenkel pairs, predicted visible defect cluster areal densities that were many of orders of magnitude below the experimentally observed values that were in the range of 0.2 to 5×10^{-3} nm^{-2}.[36] Likewise, with the assumption of spherical, isotropic reaction rate constants that follow the Smoluchowski definition in Eq. (9), it was not possible to obtain good agreement between the model predictions and the experimental results of areal defect cluster density and the observed defect cluster size distribution if the only mobile species were single vacancies and single SIA, even including the direct formation of interstitial clusters within the displacement cascade.[36] Good agreement was obtained, as shown in Fig. 2, across a range of thin foil thickness and ion flux and fluence values for 1 MeV Kr ion irradiation at a temperature of 80 °C, when incorporating defect production due to displacement cascade formation and the possible mobility of a large number of interstitial cluster defects.

However, a key uncertainty in the model was how best to parameterize the mobility of self-interstitial clusters. MD simulations have revealed both the formation of crowdion clusters in displacement cascades[9–11] as well as the very high mobility of these clusters,[15–17] which can also be thought of as prismatic dislocation loop embryo, in one-dimension along their Burgers vector. These MD observations led to the idea of the production bias model extension of the classical rate theory,[58] but experimental observations in the TEM by Arakawa and co-workers[59] have indicated that the loop migration energies are much higher than observed in the MD simulations. Arakawa further postulated that the higher activation energies for loop migration were due to the strain field interactions between the prismatic dislocation loops and interstitial type impurities within the matrix, akin to Cottrell atmosphere interactions responsible for Luders band behavior.[60] Thus, the activation energy for interstitial cluster and small interstitial cluster diffusion was treated as a fitting parameter in this work, utilizing only a subset of the experimental data. The resulting optimized interstitial cluster diffusion coefficients are presented in Table I, and the strikingly good agreement between the experimental and model predictions across two orders of magnitude of ion flux (which were not included in the parameter optimization) provides a validation of the CD model and approach, at least for irradiation temperatures around 80 °C.

Xu and co-workers also verified this CD model by comparing to OKMC simulations, as described in more

https://doi.org/10.1557/jmr.2015.25 Published online by Cambridge University Press

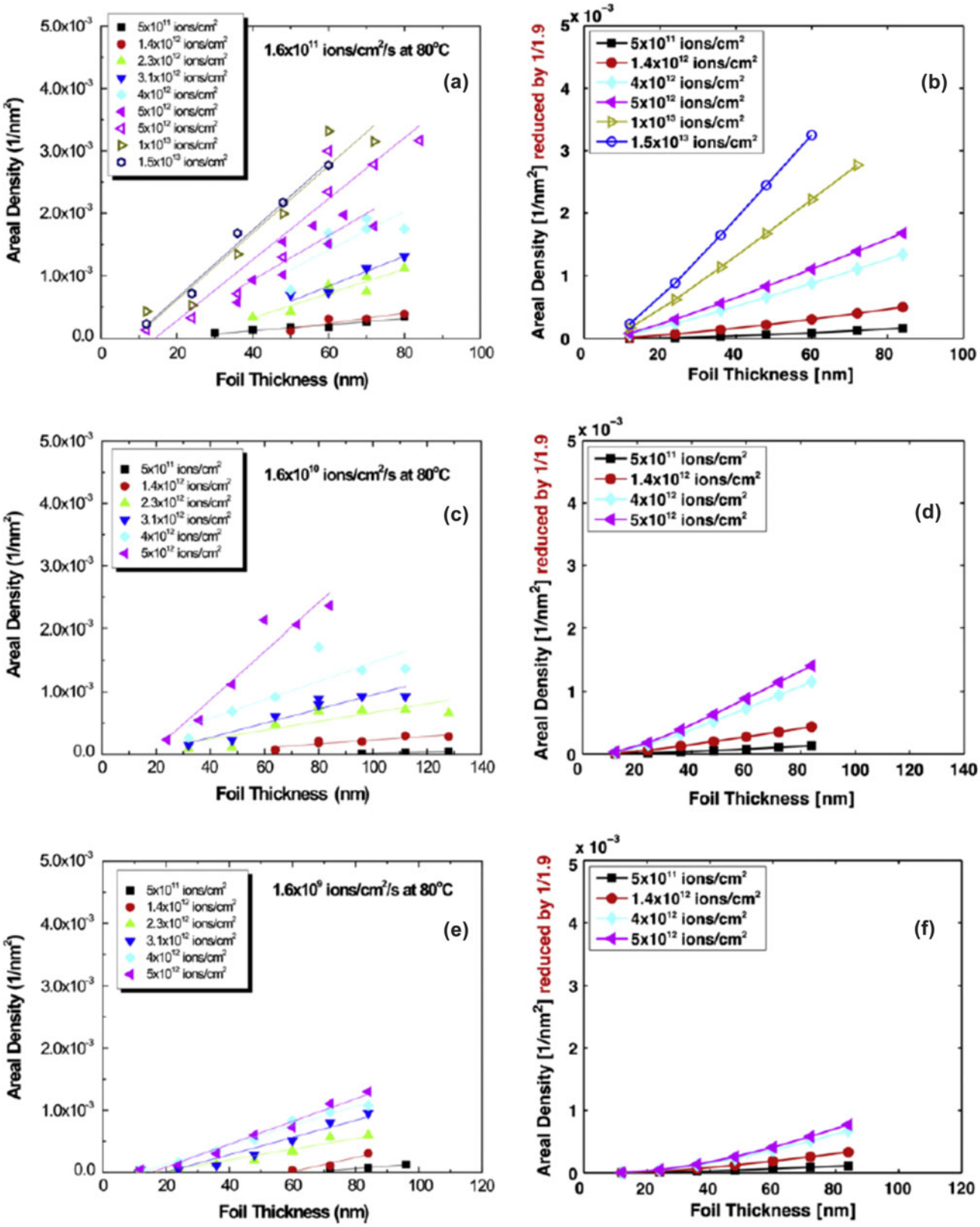


FIG. 2. Experimental (a, c, and e) and model-predicted (b, d, and f) areal density of observed loops (size greater than 1.3 nm) in molybdenum foils of varying thickness, which were irradiated with 1 MeV Kr ions to a specified flux and fluence at a temperature of approximately 80 °C.

https://doi.org/10.1557/jmr.2015.25 Published online by Cambridge University Press

detail in Ref. 41. Figure 3 compares the areal density of visible defects as a function of ion fluence obtained from OKMC and our previous spatially dependent CD model for three foil thicknesses (36, 60, and 84 nm) at three ion fluxes: 1.6×10^{11} (a), 1.6×10^{10} (b), and 1.6×10^{9} (c) ions cm^{-2} s^{-1}. Clearly, the OKMC and the CD not only predict the same qualitative trend of increasing areal density with increasing ion fluence, foil thickness, and ion flux, but they are also in excellent quantitative agreement such that the two sets of data nearly completely overlap. While not shown here, the two computational approaches also predict essentially identical size distributions of the visible defect clusters. The strong agreement between the OKMC and the CD results confirms, within the scope of effective 3-D diffusion of interstitial clusters, the numerical fidelity of the extended CD model for the study of the defect agglomeration in thin foils. Several future challenges toward modeling defect accumulation kinetics will be discussed in Sec. IV.

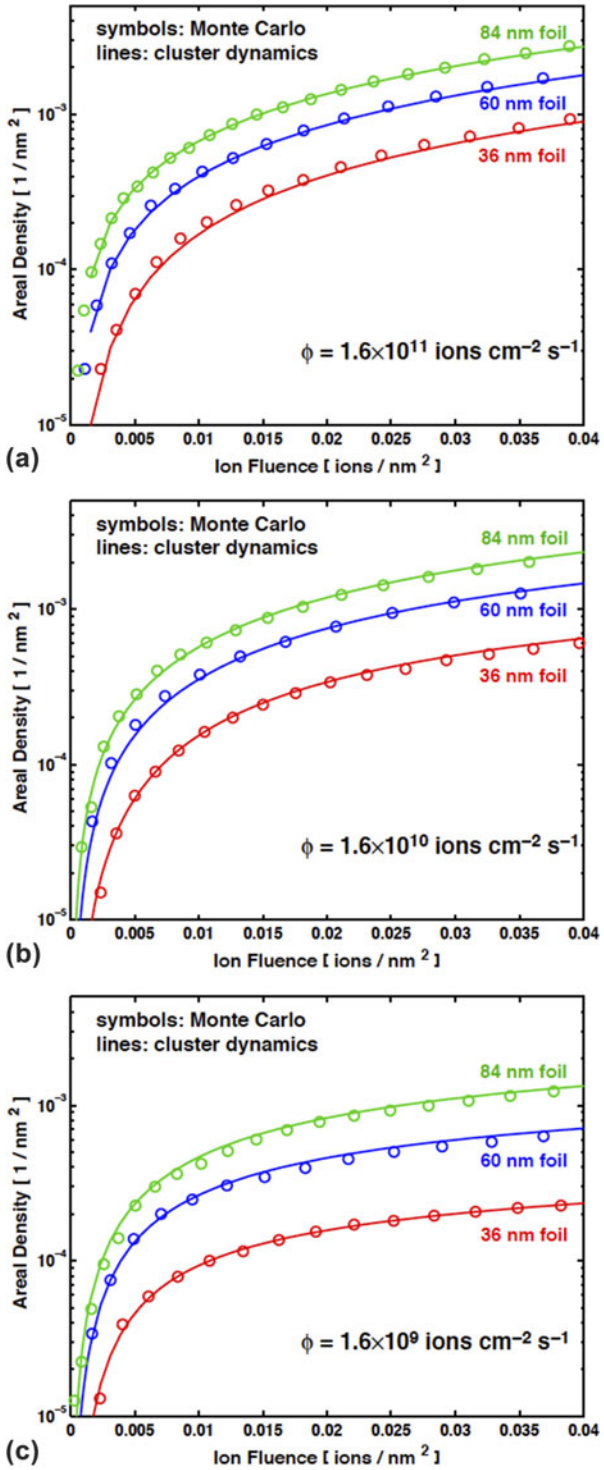


FIG. 3. Comparison of areal density of visible defects from OKMC (open symbols) versus the CD model (solid lines) for three different foil thicknesses at three ion flux levels, (a) 1.6×10^{11}, (b) 1.6×10^{10}, and (c) 1.6×10^{9} ions/cm^2/s.

B. Neutron irradiation of Fe

Hu and co-workers[40] modeled the neutron irradiation of nominally pure iron within the temperature range of 60–100 °C and compared the model predictions of black dot defect density to TEM observations, and vacancy size distribution to positron annihilation measurements. Table II presents the kinetic parameterization of vacancy and self-interstitial atom cluster diffusivity used for iron, which was based on a similar approach to that used by Xu and co-workers for molybdenum. Figure 4 presents modeling results of the vacancy and interstitial cluster distributions as a function of irradiation dose. It can be seen that interstitials undergo significant clustering at these doses and temperatures, while vacancies do not. This reflects the fact that interstitials are much more mobile than vacancies. By comparing Figs. 4(a) and 4(b), one can see that the interstitial and vacancy size distributions slightly shift to larger cluster sizes at 100 °C, indicating that both interstitial and vacancy clustering are larger at the slightly higher temperature.

Eldrup et al.[61] used PAS to obtain information on the vacancy cluster populations in pure iron after these same neutron irradiation conditions. In the quantitative analysis, the measured lifetime spectra for the irradiated Fe samples were resolved into five lifetime components, four of which have fixed lifetimes: 200, 300, 400, and 500 ps, equivalent to three dimensional vacancy clusters with a size of about 0.35, 0.54, 0.73, and >1.0 nm in diameter, respectively. The application of a positron trapping model to the measured positron lifetime spectra was used to obtain the density of different defect clusters, providing a rough size distribution of vacancy clusters in iron under various irradiation conditions, shown in Fig. 5. The output from the CD model predictions, similar to that shown in Fig. 4 but at an appropriate dose level, can be easily analyzed to extract the quantities that are acquired in the experiments so that direct comparisons can be drawn between the modeling

https://doi.org/10.1557/jmr.2015.25 Published online by Cambridge University Press

TABLE II. Mobility set to describe the diffusivity (given in terms of prefactor, D_0, and activation energy, E^m, such that $D = D_0\exp(-E^m/kT)$) for interstitial clusters and single vacancy for the modeling of neutron irradiated (nominally) pure iron.

	V	I_1–I_7	I_8	I_9	I_{10}	I_{11}	I_{12}	I_{13}	I_{14}	I_{15}	$I_{n>15}$
Diffusion prefactor, D_0 (nm^2/s)	1.37×10^{11}	$1.37 \times 10^{11}/n$									$1.37 \times 10^{11}/n^{0.7}$
Activation energy, E^m (eV)	0.75	0.34	0.45	0.50	0.55	0.65	0.75	0.80	0.9	0.95	1.1

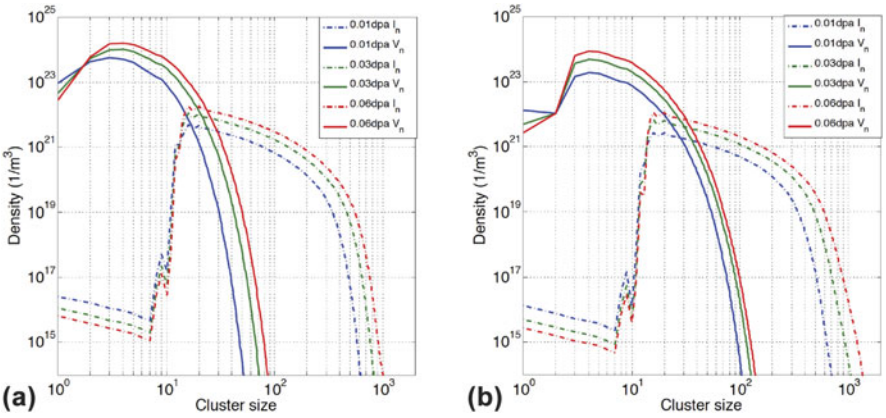


FIG. 4. Volumetric density of interstitial (solid) and vacancy (dashed) clusters predicted by the CD model as a function of cluster size (n, # of point defects contained in the cluster) at (a) 60 and (b) 100 °C, as a function of neutron dose (0.01, 0.03, and 0.06 dpa as blue, green, and red, respectively).

predictions and the PAS measurement. For example, the total volumetric density of vacancy clusters can be obtained by summing over different defects, and the size distribution can be obtained by binning the defects into various size intervals and summing the volumetric densities within each bin. In Fig. 5, the modeling results of the vacancy cluster size distributions at 60 and 100 °C are plotted together with the PAS measurements for three different irradiation doses of 0.0001, 0.0009, and 0.009 dpa. Generally, the modeling results show a similar trend of increasing density of increasing cluster sizes with increasing radiation dose, as the experimental measurements. For the neutron irradiation doses of 0.0001 and 0.0009 dpa, the PAS experimental analysis indicates that most of the vacancy clusters have a size less than 3.5 nm and the densities decrease with increasing sizes. The models reproduce these features except the modeling predictions at 0.0009 dpa at 100 °C, for which the vacancy clusters of intermediate sizes have a slightly larger volumetric density. When the neutron dose increases to 0.009 dpa, the PAS results show that the vacancy clusters with diameters in a range of 0.35–0.54 nm are dominant in the measured positron lifetime spectra, which is also in good agreement with the model predictions. Overall, the modeling predictions at these two temperatures bracket the PAS measurements and are in quite good agreement when considering the uncertainty within the experimental measurements.

The PAS measurements thus provide a comparison and verification of the vacancy cluster distribution predicted by the CD model based on reaction-diffusion rate theory. As well, it is important to validate the modeling prediction of the interstitial cluster distribution. Reference 61 describes the results of a TEM investigation on the neutron irradiated Fe samples performed to characterize the density of the interstitial type dislocation loops. It is important to note that not all interstitial clusters, but only those with a diameter exceeding the TEM resolution limit, can be observed by TEM. Further, not all dislocation loops will be resolvable in the TEM due to the $\boldsymbol{g}\cdot\boldsymbol{b}$ invisibility criteria.[43] The resolution limit in such TEM experiments varies slightly with material conditions as well as TEM operating conditions, but is generally in the range of 1.0–1.6 nm. In bcc iron, a 1.4 nm diameter corresponds to a 32-member interstitial cluster (I32) of 2-D planar shape, and a 1.6 nm diameter corresponds to I42. This implies that the comparison of the modeling results and the experimental observations will be sensitive to the choice of the TEM resolution limit. Figure 6 shows the TEM observations (in blue squares) and the modeling results at the neutron irradiation temperatures of 60 and 100 °C for four different TEM resolution limits. The simulation results are always higher than experimental data. This discrepancy could be ascribed to a combination of errors resulting from both modeling predictions and experimental observations. For the mean-field reaction-diffusion CD model, the introduction

https://doi.org/10.1557/jmr.2015.25 Published online by Cambridge University Press

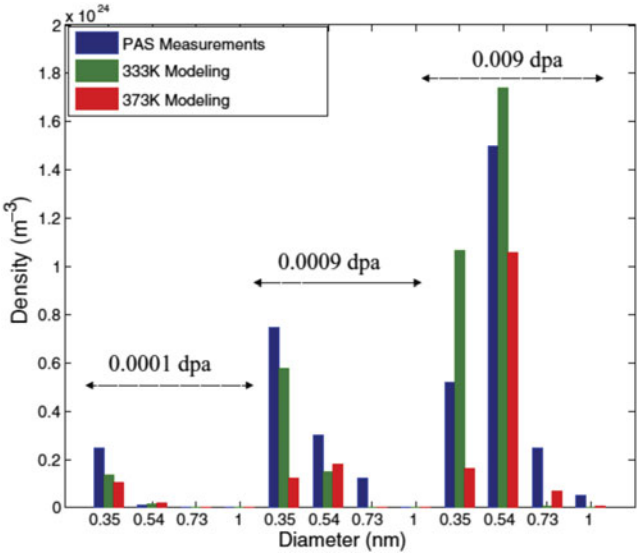


FIG. 5. Comparison of modeling predictions (at 60 and 100 °C in green and red, respectively) versus experimental positron measurements of the vacancy cluster size distribution in neutron irradiated iron, as a function of dose in dpa.

of new clusters by neutron irradiation is independent of the existing clusters. MD simulations indicate the possible reaction amongst pre-existing defect clusters and a newly produced displacement cascade, which can result in additional recombination or clustering reactions that may limit nucleation of new defect clusters. However, the MD database of cascade overlap and impact on pre-existing defect clusters is currently insufficient to appropriately model the reaction rate contant for this type of reaction, and thus, this effect is not included in the current model, which may result in a slight overestimation of defect clusters. On the other hand, not all interstitial clusters are resolvable in TEM observations due to the $\boldsymbol{g}\cdot\boldsymbol{b}$ invisibility criteria,[43] unless careful TEM characterization is done by selecting multiple g vectors and incorporating consideration of which conditions may result in SIA clusters being revealed more than once. This possible underestimation may also contribute to the discrepancy between the modeling and experimental results.

Although there are some quantitative differences between the modeling and TEM measurements, the order of the magnitude of the interstitial cluster densities is generally comparable, and within the experimental error usually estimated to be about an order of magnitude.[61,62] It is noted that the lower the TEM resolution limit (larger diameter for the smallest observable loop), the better the agreement between the experimental measurements and the modeling. Also, the modeling predictions at 100 °C agree slightly better with the experimental observations than the lower temperature of 60 °C. Another important parameter for the validation of the developed model is the average dislocation loop size, which is obtained from weighted average of visible interstitial clusters. The comparison between modeling predictions and experimental observations[62] of visible loop size is shown in Fig. 6(b) and demonstrates that a quite good agreement is achieved, especially for the higher two doses and higher temperature model predictions. Overall, the agreement observed for both the vacancy and interstitial cluster size distributions for the case of neutron irradiated iron again gives confidence in the CD modeling approach and assumptions, and Sec. IV will discuss some outstanding questions that remain to be addressed.

C. 1 MeV Kr irradiation of Fe–Cr ferritic/martensitic alloys in the IVEM

A wide variety of detailed data on the development of intermediate dose (less than ten dpa) irradiation damage microstructures in ferritic/martensitic steels and other bcc alloys has been produced by in situ ion irradiation studies.[63–69] Such experiments allow irradiation concurrent with observation in a transmission electron microscope. A black dot damage microstructure is seen to dominate irradiated ferritic/martensitic alloys up to temperatures of at least 300 °C.[63–67,70,71] At higher temperatures, extended prismatic dislocation loops with $a/2\langle 111\rangle$ or $a\langle 100\rangle$ Burgers vectors are clearly distinguished. Notably, as shown in Fig. 7, there is relatively little temperature dependence on the saturation number density either in model Fe–Cr based ferritic–martensitic alloys studied by Kaoumi and co-workers[67] or in the commercial alloy NF616 studied by Topbasi and Motta.[66,71]

The black dots, which formed at lower temperatures, are presumably also interstitial type loops of a sufficiently small size that the dislocation itself cannot be resolved. These two to five nm features become difficult to analyze because of their size, however, limiting confident assessments of type or Burgers vector. Numerous studies have indicated that these features grow in density up to a saturation value, beyond which the defect clusters grow in size at nominally constant density.[66,67] In situ experiments have provided new clues as to the properties of these defects. Under both electron and heavy ion irradiation, the thermally immobile damage features have been widely observed to undergo occasional but rapid translations spanning distances on the order of a few to several tens of nanometers which punctuate extended periods where no motion occurs at all.[64,71–74] Notably, these "hops" generally occur only when the ion or electron beam is operating and occur over the entire regime of black dot damage, even at temperatures as low as 50 K. The limited mobility of such features contrasts vividly with predictions about their motion based on MD simulations, in which interstitial clusters diffuse along

https://doi.org/10.1557/jmr.2015.25 Published online by Cambridge University Press

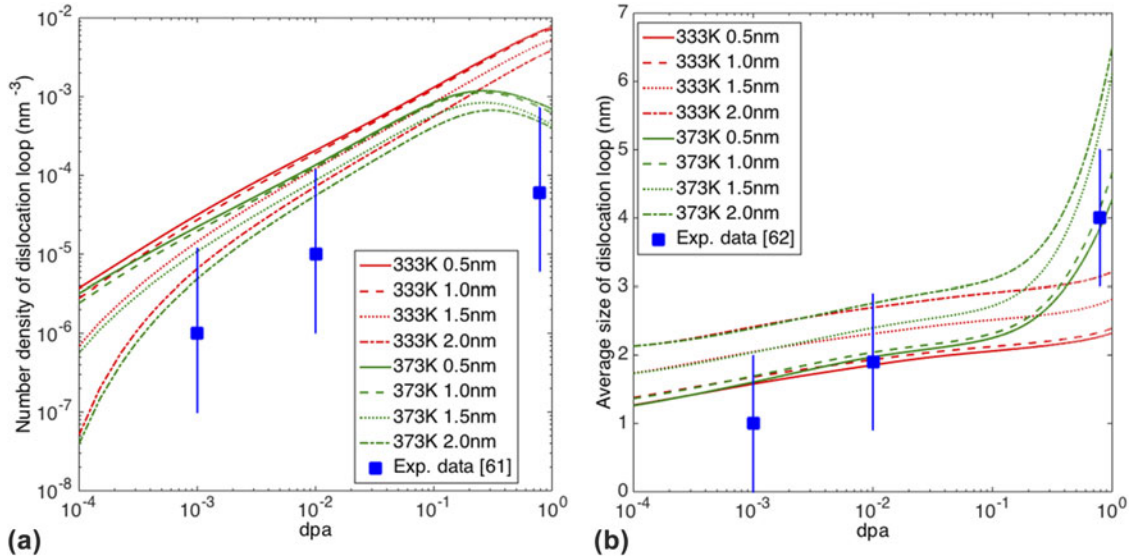


FIG. 6. Comparison of CD modeling predictions of (a) interstitial-type dislocation loop density and (b) average size of the visible dislocation loop for four different TEM resolution limits (0.5, 1.0, 1.5, and 2.0 nm) at two different neutron irradiation temperatures for the Fe-a samples, as compared to the TEM observations of Refs. 61 and 62.

one-dimensional trajectories with very low (less than 0.1 eV) activation energies.[15–17] The reconciliation of disparate expected and observed behaviors has been rationalized by "traps", broadly defined as a variety of impurities or impurity defect complexes which bind to the dislocation loops and lower their mobility. Though multiple candidates for the composition of such traps have been proposed, trapping has been invoked to explain the lower than expected thermal mobility of loops[15] as well as the hops seen in irradiation environments.[72,73]

Kohnert[45,46] has included a beam-assisted mobility to account for the aforementioned "hops" of black dot defects during the in situ ion irradiations, by modeling the diffusivity of interstitial clusters within the CD framework described in Eqs. (1)–(10), as:

$$D = D_0 e^{-E^m/kT} + \frac{\lambda_{irr}}{2N}\nu_{irr} \quad , \qquad (11)$$

where the first term describes the normal Arrhenius type diffusion and the second term describes the dynamic behavior observed during in situ experiments where thermally immobile (presumably trapped) loops undergo occasional but rapid translations. Presumably, this erratic motion during the ion irradiation is due to a series of ballistic de-trapping events induced by energetic recoils. The effective diffusivity due to such ballistic motion is described with an activation frequency, ν_{irr}, and a discrete hop length, λ_{irr}, which describes the effective distance between hops as determined by the concentration of impurity traps, and where N is the dimensionality of diffusion (assumed to be three-dimensional based on observed erratic nature of the motion).

Figure 8 demonstrates the CD model predictions for 1 MeV Kr ion irradiation of ferritic–martensitic alloys, as compared to the saturation density observed by Kaoumi et al.[67] and Topbasi et al.[66,71] Here, the thermal diffusion of large interstitial clusters is based on an activation energy of 1.3 eV, consistent with in situ TEM observations of Arakawa,[59] as discussed earlier. The activation energies for the single interstitial and small interstitial clusters are set equal to values obtained from ab initio calculations,[75,76] while all interstitial clusters greater than size 3 are set to the saturation value of 1.3 eV (Model I). There are subtle differences between Models I and II in terms of the activation energy of the small interstitial clusters, wherein Model I uses a value of 1.3 eV for all interstitial clusters larger than size 3, whereas Model II sets the migration energy for interstitial clusters between 4 and 9 to linearly increase with size, and then sets all clusters greater than size 9 to the saturation value of 1.3 eV.[75] Thus, Model II is similar to the optimization approach to setting the activation energy of small interstitial clusters taken by Xu et al.[36,39–43] Notably, when the beam-assisted diffusion term, Eq. (11), was not included, the predicted areal defect density did not saturate but experiences breakaway growth. As shown in Fig. 8, both Models I and II predict a temperature dependence of the defect cluster saturation density that is consistent with the experimental observations. This can be rationalized due to the nucleation and growth behavior of the defect cluster density and the fact that the beam assisted diffusivity provides a

https://doi.org/10.1557/jmr.2015.25 Published online by Cambridge University Press

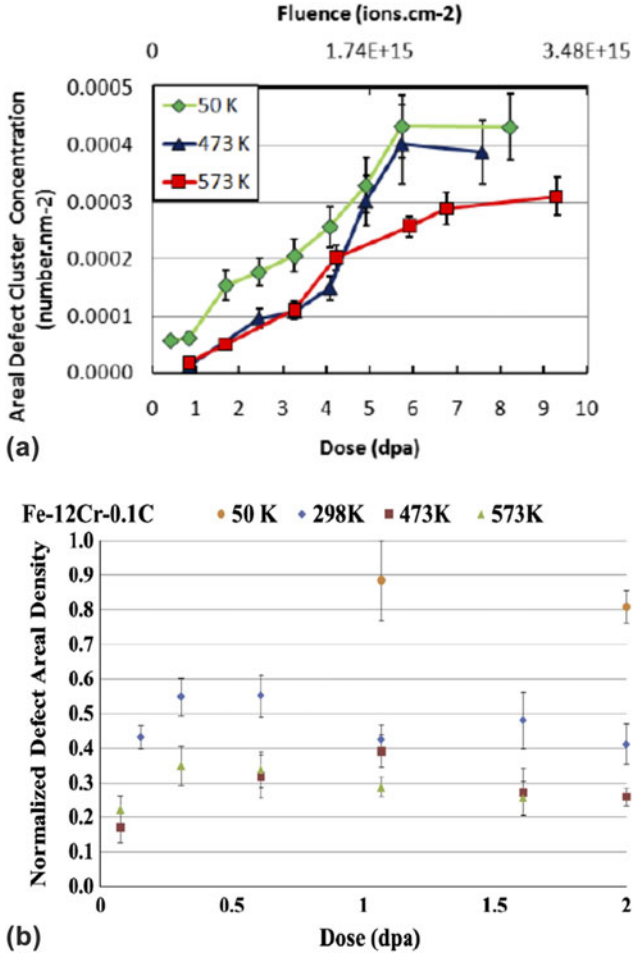


FIG. 7. Temperature dependence of the areal defect density as a function of radiation dose for 1 MeV Kr ion irradiation of (a) commercial alloy NF616 (Refs. 66 and 71) and (b) a model ferritic–martensitic steel with nominal composition of Fe–12Cr–0.1C, where the defect density has been normalized to the highest measured density at 50 K.[67]

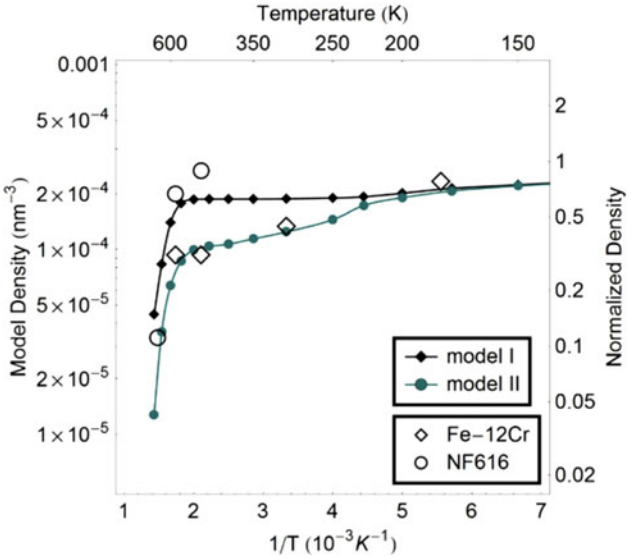


FIG. 8. Predicted saturation density of visible defect clusters for 1 MeV Kr ion irradiation of ferritic–martensitic alloys from the CD model with beam activated diffusion implemented in the form of Eq. (11). The experimental data from Fig. 7 (Refs. 66, 67, and 71) are shown for comparison, as normalized to the defect density at 50 K.

mechanism for cluster sizes which would otherwise be thermally immobile to interact with each other.

IV. DISCUSSION OF OUTSTANDING ISSUES

In this article, we have provided a review of three recent modeling studies that have compared reaction-diffusion based CD models to in situ TEM studies of the defect accumulation during 1 MeV Kr ion irradiation of nominally pure molybdenum or ferritic–martensitic steels, in addition to neutron irradiation of nominally pure iron. Overall, the agreement between the modeling predictions and the experiments is quite good and demonstrates an impressive ability to capture the multiscale nature of radiation effects on structural materials, at least in terms of the evolution of the interstitial defect clusters which develop into the black dot structure of prismatic dislocation loops in bcc materials at intermediate radiation temperature, as well as the subvisible vacancy cluster distribution in neutron irradiated iron. Indeed, the in situ TEM irradiation experiments provide a unique opportunity to examine the fine details of defect evolution under continuous irradiation, and, when combined with CD modeling, provide a nice opportunity to verify fundamental assumptions/uncertainties with respect to damage production and kinetics/energetics of irradiation defects.

While the results presented here do provide a good agreement with the experimental observations, there are a number of assumptions inherent in these modeling results, which merit further investigation. First and foremost is the assumption of the isotropic three-dimensional reaction kinetics that underpin the Smoluchowski reaction rate constants of Eq. (9). Kohnert has begun to investigate this assumption in detail, as Barashev and co-workers.[77] However, the mathematical formulations rapidly become quite complex within models that have multiple diffusing species, as is necessary to treat the prismatic interstitial loop behavior in real-world materials containing impurities, and for which the resulting migration behavior is presumably determined trapping and de-trapping interactions. While the effective isotropic diffusion assumed within the modeling results presented from Xu on the defect cluster evolution in molybdenum[36,41–43] and Hu for the neutron irradiation results in iron[40] is quite impressive, clearly these models need to be validated by comparison with experimental data across a much wider temperature regime. Thus, there is a need for additional, high-fidelity experimental

https://doi.org/10.1557/jmr.2015.25 Published online by Cambridge University Press

characterization of the defect cluster microstructure in irradiated materials with irradiation temperatures ranging from below Stage III to near Stage V to validate the defect cluster diffusion kinetics and reaction rate constants that are inherent to the reaction-diffusion CD, or OKMC modeling approaches.

Future modeling and experimental studies are also needed to further understanding of the interactions amongst defect clusters and with extended microstructural sinks. For example, there remain numerous unresolved questions about defect cluster evolution as the result of cascade overlap and about the quantitative details in how we treat the reaction rate densities between defect clusters and various microstructural sinks, including dislocations, grain boundaries, nanometer-sized precipitate interfaces, as well as reactions amongst the defect clusters themselves. The quantification of the sink efficiency of dislocations, free surfaces or grain boundaries with radiation dose, and how variations may relate to the absorption of vacancy versus interstitial defects, is another example of an outstanding question that has been postulated to be responsible for the swelling response of irradiated materials.

Another import aspect of the visible defect cluster evolution is the identity of the Burgers vector of the visible loop populations. It is well established that in iron and other bcc materials, some portion of the prismatic loop population following irradiation has Burgers vector of $a\langle 100\rangle$, and in some cases, the fraction of $\langle 100\rangle$ loops is dominant. In the modeling presented here, no discrimination has been made between possible $a/2\langle 111\rangle$ and $a\langle 100\rangle$ dislocation loops since this would require parameterization of cluster type to evaluate the multiple models that have been proposed in the literature to explain the $a\langle 100\rangle$ loop formation. However, this is a topic which the models should be able to address in the near future, especially given the continual increases in computational capability and memory required to treat ever larger reaction networks. Such modeling efforts would be further complemented by additional detailed microscopy to expand the database of loop populations as a function of irradiation conditions and the type of bcc material.

The results presented here are also limited to rather small radiation damage levels below a few displacements per atom. As noted by Li and co-workers in describing the experimental observations in Mo[43] and by Kaoumi and co-workers in the ferritic–martensitic alloys,[67] at higher doses, a pronounced rafting or spatial arrangement was observed in the visible defect cluster distributions. This has not been captured within the current models, which are limited to one spatial dimension, and for which elastic interactions amongst the defect clusters and other microstructural features are not included. But, clearly, this is another need for coordinated modeling and experimental studies in the future. It can be further supposed that the observed dislocation loop rafting behavior may be responsible for the saturation of the mechanical properties that is observed at higher doses in structural materials. Unraveling this will require a combination of spatially resolved, e.g., tomographic, studies of the evolution of the defect cluster distributions across a range of radiation exposures and temperatures, coordinated with extensions of the multiscale modeling methodology to specifically investigate the role of elastic interactions amongst defect populations to describe such higher dose behavior.

Finally, the modeling results here have focused entirely on the evolution of vacancy and interstitial type defect clusters in irradiated bcc materials, without any consideration of the coupling of the defect and solute/impurity fluxes. There is a long-standing literature on the radiation induced segregation in austenitic alloys as well as more recent work on radiation-induced segregation in ferritic–martensitic materials. This article has not attempted to review that literature, other than to note that this is an area which is receiving increasing attention toward coupling the defect and solute fluxes which occur under irradiation to thermodynamic predictions of radiation-induced phase formation.

V. SUMMARY

As highlighted here, CD models provide a powerful reaction-diffusion rate theory based modeling approach that allows high fidelity calculations of the density of irradiation induced defects and their contributions to long term microstructural evolution. This article has reviewed three recent applications of CD models, including the verification of the computational fidelity of the model against OKMC models, which predict the visible defect cluster distributions that evolve in molybdenum, iron, and ferritic–martensitic alloys up to radiation dose levels on the order of a few displacements per atom. We have also identified several areas that require further coordinated experimental characterization and modeling, including the diffusivity and reaction kinetics of small interstitial clusters in bcc materials, the evaluation of the multiple models to rationalize the formation of prismatic loops with $a\langle 100\rangle$ Burgers vectors in irradiated bcc materials, and the formation of spatial arrangements, or rafts, of dislocation loops which is observed at higher radiation doses.

ACKNOWLEDGMENTS

The authors thank our experimental collaborators, Djamel Kaoumi, Cem Topbasi, and Arthur Motta for helpful discussions and gratefully acknowledge financial support from the U.S. Department of Energy, Office of Fusion Energy Sciences under grant

https://doi.org/10.1557/jmr.2015.25 Published online by Cambridge University Press

DOE-DE-SC0006661 and the U.S. Department of Energy, Office of Nuclear Energy, Nuclear Energy University Programs (NEUP).

REFERENCES

1. G.R. Odette, B.D. Wirth, D.J. Bacon, and N.M. Ghoneim: Multiscale-multiphysics modeling of radiation-damaged materials: Embrittlement of pressure vessel steels. *MRS Bull.* **26**, 176 (2001).
2. E.E. Bloom: The challenge of developing structural materials for fusion power systems. *J. Nucl. Mater.* **258–263**, 7 (1998).
3. E.E. Bloom, N. Ghoneim, R. Jone, R. Kurtz, G.R. Odette, A. Rowecliffe, D. Smith, and F.W. Wiffen: Advanced Materials Program, appendix D of the VLT roadmap. (1999). Available at http://vlt.ucsd.edu/.
4. S.J. Zinkle and N.M. Ghoniem: Operating temperature windows for fusion reactor structural materials. *Fusion Eng. Des.* **51–52**, 55 (2000).
5. T. Muroga, M. Gasparotto, and S.J. Zinkle: Overview of materials research for fusion reactors. *Fusion Eng. Des.* **61–62**, 13 (2002).
6. M. Victoria, N. Baluc, C. Bailat, Y. Dai, M.I. Luppo, R. Schaublin, and B.N. Singh: The microstructure and associated tensile properties of irradiated fcc and bcc metals. *J. Nucl. Mater.* **276**, 114 (2000).
7. T. Diaz de la Rubia, H.M. Zbib, T.A. Khraishi, B.D. Wirth, M. Victoria, and M.J. Caturla: Multiscale modelling of plastic flow localization in irradiated materials. *Nature* **406**, 871 (2000).
8. B.D. Wirth, G.R. Odette, J. Marian, L. Ventelon, J.A. Young, and L.A. Zepeda-Ruiz: Multiscale modeling of radiation damage in Fe-based alloys in the fusion environment. *J. Nucl. Mater.* **329–333**, 103 (2004).
9. G.J. Ackland, D.J. Bacon, A.F. Calder, and T. Harry: Computer simulation of point defect properties in dilute Fe–Cu alloy using a many-body interatomic potential. *Philos. Mag. A* **75**, 713 (1997).
10. R.E. Stoller, G.R. Odette, and B.D. Wirth: Primary damage formation in bcc iron. *J. Nucl. Mater.* **251**, 49 (1997).
11. W.J. Phythian, R.E. Stoller, A.J.E. Foreman, A.F. Calder, and D.J. Bacon: A comparison of displacement cascades in copper and iron by molecular dynamics and its application to microstructural evolution. *J. Nucl. Mater.* **223**, 245 (1995).
12. J.B. Gibson, A.N. Goland, M. Milgram, and G.H. Vineyard: Dynamics of radiation damage. *Phys. Rev.* **120**, 1229 (1960).
13. R.S. Averback and T. Diaz de la Rubia: Displacement damage in irradiated metals and semiconductors. *Solid State Phys.* **51**, 281 (1998).
14. W. Setyawan, G. Nandipati, K.J. Roch, H.L. Heinisch, B.D. Wirth, and R.J. Kurtz: Displacement cascades and defects annealing in tungsten, Part I: Defect database from molecular dynamics simulations. *J. Nucl. Mater.* (2015, in press). doi:10.1016/j.jnucmat.2014.12.056.
15. N. Soneda and T. Diaz de la Rubia: Defect production, annealing kinetics and damage evolution in α-Fe: An atomic-scale computer simulation. *Philos. Mag. A* **78**, 995 (1998).
16. B.D. Wirth, G.R. Odette, D. Maroudas, and G.E. Lucas: Dislocation loop structure, energy and mobility of self-interstitial atom clusters in bcc iron. *J. Nucl. Mater.* **276**, 33 (1999).
17. N. Anento, A. Serra, and Y.N. Osetsky: Atomistic study of multi-mechanism diffusion by self-interstitial defects in α-Fe. *Model. Simul. Mater. Sci. Eng.* **18**, 025008 (2010).
18. B.D. Wirth, G.R. Odette, and R.E. Stoller: Recent progress toward an integrated multiscale-multiphysics model of reactor pressure vessel embrittlement, in *Advances in Materials Theory and Modeling–Bridging over Multiple-length and Time Scales* (*Mater. Res. Soc. Symp. Proc.* **677**, San Francisco, CA, 2001) 677-AA5.2.
19. H.L. Heinisch and B.N. Singh: Stochastic annealing simulation of intracascade defect interactions. *J. Nucl. Mater.* **251**, 77 (1997).
20. M.J. Caturla, N. Soneda, E.A. Alonso, B.D. Wirth, and T. Diaz de la Rubia: Comparative study of radiation damage accumulation in Cu and Fe. *J. Nucl. Mater.* **276**, 13 (2000).
21. P.R. Monasterio, B.D. Wirth, and G.R. Odette: Kinetic Monte Carlo modeling of cascade aging and damage accumulation in Fe–Cu alloys. *J. Nucl. Mater.* **361**, 127 (2007).
22. G. Nandipati, W. Setyawan, H.L. Heinisch, K.J. Roche, R.J. Kurtz, and B.D. Wirth: Displacement cascades and defect annealing in tungsten, Part II: Object kinetic Monte Carlo simulation of tungsten cascade aging. *J. Nucl. Mater.* (2015, in press). doi: http://dx.doi.org/10.1016/j.nucmat.2014.09.067.
23. M. Eldrup and B.N. Singh: Void nucleation in fcc and bcc metals: A comparison of neutron irradiated copper and iron. *Mater. Sci. Forum* **363–365**, 79 (2001).
24. B.D. Wirth, G.R. Odette, P. Asoka-Kumar, R.H. Howell, and P.A. Sterne: Characterization of nanostructural features in irradiated reactor pressure vessel model alloys. In *Proceedings of the 10th International Symposium on Environmental Degradation of Materials in Light Water Reactors*, G.S. Was ed.; National Association of Corrosion Engineers 2002.
25. G.R. Odette: On mechanisms controlling swelling in ferritic and martensitic alloys. *J. Nucl. Mater.* **155–157**, 921 (1988).
26. H. Matsui, K. Fukumoto, D.L. Smith, H.M. Chung, W. van Witzenburg, and S.N. Votinov: Status of vanadium alloys for fusion reactors. *J. Nucl. Mater.* **233–237**, 92 (1996).
27. R. Schaublin, P. Spatig, and M. Victoria: Microstructure assessment of the low activation ferritic/martensitic steel F82H. *J. Nucl. Mater.* **258–263**, 1178 (1998).
28. A.F. Rowcliffe, J.P. Robertson, R.L. Klueh, K. Shiba, D.J. Alexander, M.L. Grossbeck, and S. Jitsukawa: Fracture toughness and tensile behavior of ferritic–martensitic steels irradiated at low temperatures. *J. Nucl. Mater.* **258–263**, 1275 (1998).
29. P. Spatig, R. Schaublin, S. Gyger, and M. Victoria: Evolution of the mechanical properties of the F82H ferritic/martensitic steel after 590 MeV proton irradiation. *J. Nucl. Mater.* **258–263**, 1345 (1998).
30. R. Schaublin, P. Spatig, and M. Victoria: Chemical segregation behavior of the low activation ferritic/martensitic steel F82H. *J. Nucl. Mater.* **258–263**, 1350 (1998).
31. D.S. Gelles, P.M. Rice, S.J. Zinkle, and H.M. Chung: Microstructural examination of irradiated V–(4–5%)Cr–(4–5%)Ti. *J. Nucl. Mater.* **258–263**, 1380 (1998).
32. P.M. Rice and S.J. Zinkle: Temperature dependence of the radiation damage microstructure in V–4Cr–4Ti neutron irradiated to low dose. *J. Nucl. Mater.* **258–263**, 1414 (1998).
33. J. Gazda, M. Meshii, and H.M. Chung: Microstructure of V–4Cr–4Ti alloy after low-temperature irradiation by ions and neutrons. *J. Nucl. Mater.* **258–263**, 1437 (1998).
34. E.V. van Osch and M.I. De Vries: Irradiation hardening of V–4Cr–4Ti. *J. Nucl. Mater.* **271–272**, 162 (1999).
35. Y. Candra, K. Fukumoto, A. Kimura, and H. Matsui: Microstructural evolution and hardening of neutron irradiated vanadium alloys at low temperatures in Japan Material Testing Reactor. *J. Nucl. Mater.* **271–272**, 301 (1999).
36. D.H. Xu, B.D. Wirth, M.M. Li, and M.A. Kirk: Combining in situ transmission electron microscopy irradiation experiments with cluster dynamics modeling to study nanoscale defect agglomeration in structural metals. *Acta Mater.* **60**, 4286 (2012).
37. D. Xu and B.D. Wirth: Spatially dependent rate theory modeling of thermal desorption spectrometry of helium-implanted iron. *Fusion Sci. Technol.* **56**, 1064 (2009).

https://doi.org/10.1557/jmr.2015.25 Published online by Cambridge University Press

38. D. Xu and B.D. Wirth: Modeling spatially dependent kinetics of helium desorption in BCC iron following He ion implantation. *J. Nucl. Mater.* **403**, 184 (2010).
39. D. Xu, X. Hu, and B.D. Wirth: A phase-cut method for multi-species kinetics: Sample application to nanoscale defect cluster evolution in alpha iron following helium ion implantation. *Appl. Phys. Lett.* **102**, 011904 (2013).
40. X. Hu, D. Xu, T.S. Byun, and B.D. Wirth: Modeling of irradiation hardening of iron after low-dose and low-temperature neutron irradiation. *Model. Simul. Sci. Eng.* **22**, 0655002 (2014).
41. D. Xu, B.D. Wirth, M. Li, and M.A. Kirk: Defect microstructural evolution in ion irradiated metallic nanofoils: Kinetic Monte Carlo simulation versus cluster dynamics modeling and in situ transmission electron microscopy experiments. *Appl. Phys. Lett.* **101**, 101905 (2012).
42. D. Xu, B.D. Wirth, M. Li, and M.A. Kirk: Recent work towards understanding defect evolution in thin molybdenum foils through in situ ion irradiation under TEM and coordinated cluster dynamics modeling. *Curr. Opin. Solid State Mater. Sci.* **16**, 109 (2012).
43. M. Li, M.A. Kirk, P.M. Baldo, D. Xu, and B.D. Wirth: Study of defect evolution by TEM with in situ ion irradiation and coordinated modeling. *Philos. Mag.* **92**(16), 2048 (2012).
44. C.S. Becquart and B.D. Wirth: Kinetic Monte Carlo simulations of irradiation effects. In *Comprehensive Nuclear Materials*, Elsevier, 2012, Chapter 1.14.
45. A.A. Kohnert and B.D. Wirth: *Phys. Rev. B* (2014, submitted).
46. A.A. Kohnert: The kinetics of dislocation loop formation in ferritic alloys through the aggregation of irradiation induced defects. Ph.D. Thesis, University of California, Berkeley, 2014.
47. C.J. Ortiz and M.J. Caturla: Simulation of defect evolution in irradiated materials: Role of intracascade clustering and correlated recombination. *Phys. Rev. B* **75**, 184101 (2007).
48. C.J. Ortiz, P. Pichler, T. Fuhner, F. Cristiano, B. Colombeau, N.E.B. Cowern, and A. Claverie: A physically based model for the spatial and temporal evolution of self-interstitial agglomerates in ion implanted silicon. *J. Appl. Phys.* **96**, 4866 (2004).
49. M.V. Smoluchowski: A mathematical theory of coagulation kinetics of colloidal solutions. *Z. Phys. Chem.* **92**, 192 (1917).
50. T.R. Waite: Theoretical treatment of the kinetics of diffusion-limited reactions. *Phys. Rev. B* **107**, 463 (1957).
51. H.L. Heinisch, B.N. Singh, and S.I. Golubov: The effects of one-dimensional glide on the reaction kinetics of interstitial clusters. *J. Nucl. Mater.* **283**, 737 (2000).
52. H.L. Heinisch, H. Trinkaus, and B.N. Singh: Kinetic Monte Carlo studies of the reaction kinetics of crystal defects that diffuse one-dimensionally with occasional transverse migration. *J. Nucl. Mater.* **367–370**, 332 (2007).
53. P. Erhart and J. Marian: Calculation of the substitutional fraction of ion-implanted He in an α-Fe target. *J. Nucl. Mater.* **414**, 426 (2011).
54. R.E. Stoller, S.I. Golubov, C. Domain, and C.S. Becquart: Mean field rate theory and object kinetic Monte Carlo: A comparison of kinetic models. *J. Nucl. Mater.* **382**, 77 (2008).
55. J.F. Ziegler, J.P. Biersack, and U. Littmark: *The Stopping and Range of Ions in Matter* (Pergamon, New York, 1984).
56. P.M. Derlet, D. Nguyen-Manh, and S.L. Dudarev: Multiscale modeling of crowdion and vacancy defects in body-centered-cubic transition metals. *Phys. Rev. B* **76**, 054107 (2007).
57. A.B. Bortz, M.H. Kalos, and J.L. Lebowitz: New algorithm for Monte-Carlo simulations of Ising spin systems. *J. Comp. Phys.* **17**, 10 (1975).
58. C.H. Woo and B.N. Singh: Production bias due to clustering of point defects in irradiation-induced cascades. *Philos. Mag. A* **65**, 889 (1992).
59. K. Arakawa, K. Ono, M. Isshiki, K. Mimura, M. Uchikoshi, and H. Mori: Observation of the one-dimensional diffusion of nanometer-sized dislocation loops. *Science* **318**, 956 (2007).
60. A.H. Cottrell: Dislocation theory of yielding and strain ageing of iron. *Proc. Phys. Soc.* **62**, 49 (1949).
61. M. Eldrup, B.N. Singh, S.J. Zinkle, T.S. Byun, and K. Farrell: Dose dependence of defect accumulation in neutron irradiated copper and iron. *J. Nucl. Mater.* **307–311**, 912 (2002).
62. S.J. Zinkle and B.N. Singh: Microstructure of neutron-irradiated iron before and after tensile deformation. *J. Nucl. Mater.* **351**, 269 (2006).
63. M. Hernandez-Mayoral, Z. Yao, M.L. Jenkins, and M.A. Kirk: Heavy-ion irradiations of Fe and Fe–Cr model alloys Part 2: Damage evolution in thin-foils at higher doses. *Philos. Mag.* **88**, 2881 (2008).
64. Z. Yao, M. Hernandez-Mayoral, M. Jenkins, and M.A. Kirk: Heavy-ion irradiations of Fe and Fe–Cr model alloys Part 1: Damage evolution in thin-foils at lower doses. *Philos. Mag.* **88**, 2851 (2008).
65. Z. Yao, M. Jenkins, M. Hernandez-Mayoral, and M.A. Kirk: The temperature dependence of heavy-ion damage in iron: A microstructural transition at elevated temperatures. *Philos. Mag.* **90**, 4623 (2010).
66. C. Topbasi, A.T. Motta, and M.A. Kirk: In situ study of heavy ion induced radiation damage in NF616 (P92) alloy. *J. Nucl. Mater.* **425**, 48 (2012).
67. D. Kaoumi, J. Adamson, and M. Kirk: Microstructure evolution of two model ferritic/martensitic steels under in situ ion irradiation at low doses (0–2 dpa). *J. Nucl. Mater.* **445**, 12 (2014).
68. M.A. Kirk, P.M. Baldo, A.C. Liu, E.A. Ryan, R.C. Birtcher, Z. Yao, S. Xu, M.L. Jenkins, M. Hernandez-Mayoral, D. Kaoumi, and A.T. Motta: In situ transmission electron microscopy and ion irradiation of ferritic materials. *Microsc. Res. Tech.* **72**, 82 (2009).
69. M. Jenkins, Z. Yao, M. Hernndez-Mayoral, and M. Kirk: Damage development in FeCr alloys under heavy-ion irradiation by IVEM. *J. Nucl. Mater.* **389**, 197 (2009).
70. M.L. Jenkins, C.A. English, and B.L. Eyre: Heavy-ion irradiation of alpha-iron. *Philos. Mag. A* **38**, 97 (1978).
71. C. Topbasi: Microstructural evolution of ferritic-martensitic steels under heavy ion irradiation. Ph.D. Thesis, Pennsylvania State University, 2014.
72. Y. Satoh and H. Matsui: Obstacles for one-dimensional migration of interstitial clusters in iron. *Philos. Mag.* **89**, 1489 (2009).
73. T. Hamaoka, Y. Satoh, and H. Matsui: One-dimensional motion of interstitial clusters in iron-based binary alloys observed using a high-voltage electron microscope. *J. Nucl. Mater.* **433**, 180 (2013).
74. K. Arakawa, H. Mori, and K. Ono: Formation process of dislocation loops in iron under irradiations with low-energy helium, hydrogen ions or high-energy electrons. *J. Nucl. Mater.* **307–311**, 272 (2002).
75. C.C. Fu, J.D. Torre, F. Willaime, J.L. Bocquet, and A. Barbu: Multiscale modeling of defect kinetics in irradiated iron. *Nat. Mater.* **4**, 68 (2005).
76. C.C. Fu, F. Willaime, and P. Ordejon: Stability and mobility of mono- and di-interstitials in alpha-Fe. *Phys. Rev. Lett.* **92**, 175503 (2004).
77. A.V. Barashev, S.I. Golubov, Y.N. Osetsky, and R.E. Stoller: Reaction kinetics of non-localised particle–trap complexes. *Philos. Mag.* **90**, 897 (2010).

https://doi.org/10.1557/jmr.2015.25 Published online by Cambridge University Press